OPEN ACCESS
IOP Publishing
Journal of Physics: Condensed Matter
J. Phys.: Condens. Matter **36** (2024) 383001 (11pp)
https://doi.org/10.1088/1361-648X/ad5246

Topical Review

Quantum transport in InSb quantum well devices: progress and perspective

Zijin Lei[1,2], Erik Cheah[1,2], Rüdiger Schott[1,2], Christian A Lehner[1,2], Uli Zeitler[3,4], Werner Wegscheider[1,2], Thomas Ihn[1,2] and Klaus Ensslin[1,2,*]

[1] Solid State Physics Laboratory, ETH Zurich, CH-8093 Zurich, Switzerland
[2] Quantum Center, ETH Zurich, CH-8093 Zurich, Switzerland
[3] High Field Magnet Laboratory (HFML-EMFL), Radboud University, Toernooiveld 7, 6525 ED Nijmegen, The Netherlands
[4] Institute for Molecules and Materials, Radboud University, Heyendaalseweg 135, 6525 AJ Nijmegen, The Netherlands

E-mail: ensslin@phys.ethz.ch

Received 13 March 2024, revised 24 May 2024
Accepted for publication 30 May 2024
Published 24 June 2024

Abstract

InSb, a narrow-band III–V semiconductor, is known for its small bandgap, small electron effective mass, high electron mobility, large effective g-factor, and strong spin-orbit interactions. These unique properties make InSb interesting for both industrial applications and quantum information processing. In this paper, we provide a review of recent progress in quantum transport research on InSb quantum well devices. With advancements in the growth of high-quality heterostructures and micro/nano fabrication, quantum transport experiments have been conducted on low-dimensional systems based on InSb quantum wells. Furthermore, ambipolar operations have been achieved in undoped InSb quantum wells, allowing for a systematic study of the band structure and quantum properties of p-type narrow-band semiconductors. Additionally, we introduce the latest research on InAsSb quantum wells as a continuation of exploring physics in semiconductors with even narrower bandgaps.

Keywords: InSb, quantum wells, quantum transport, InAsSb

1. Introduction

Among III–V binary compound semiconductors, InSb stands out for its small band gap (∼235 meV at 0 K) [1], the smallest effective electron mass (∼0.014 m_e in the bulk, where $m_e = 9.109 \times 10^{-31}$ kg is the free electron mass) [2], the highest room temperature mobility [3], the largest spin-orbit interaction (SOI) [4–7], and the largest effective g-factor ($|g^*| \sim 50$) in the conduction band [8]. These distinctive properties make InSb of special interest for, for example, high-speed electronics [9], optoelectronics in the infrared [10], and spintronic applications [11]. Beyond these relevant application perspectives, the unique properties of InSb also make it highly suitable for quantum transport studies at low temperatures. For instance, the small effective mass enables the observation of quantum states at relatively higher temperatures, and the large g-factor makes Zeeman effects distinctively pronounced already in a moderate magnetic field. Recently, together with InAs, research on quantum transport in InSb has been intensified because of its potential to work as a platform for topological quantum information processing. By finely tuning the Zeeman energy, chemical potential, and Rashba SOI in a 1D semiconductor coupled with an s-wave superconductor, a

* Author to whom any correspondence should be addressed.

topological nontrivial phase can be induced [12]. Furthermore, in comparison with the 1D devices, 2D systems offer greater versatility in topological applications, because the phase of superconductors can be tuned as another degree of freedom in novel devices such as Josephson junctions and SQUIDs [13–20].

In comparison to free-standing InSb materials like nanowires [21–24] and nanoflakes [25–28], InSb quantum well (QW) structures have the advantage of achieving higher electron mobility. InSb QWs with the highest mobility for quantum transport experiments are grown with advanced molecular beam epitaxy (MBE) method. However, progress in InSb QWs has faced challenges in material growth and difficulties in micro/nano fabrication. Recent advancements in MBE growth techniques for high-quality InSb QWs and the increasing reliability of InSb QW processing methods have facilitated the study of the unique properties of InSb in quantum transport devices.

In this review, we first provide a brief overview of recent progress in MBE growth of InSb QWs, where carefully designed buffer systems are applied to overcome the lattice mismatch between InSb and substrate materials. With advancements in growth and micro/nano fabrication, gate tunability of the 2DEG in InSb QWs has been achieved. High-quality InSb QW devices allow a systematic study of InSb through magneto-transport characterization. This includes verification of the small effective mass, the large effective g-factor, and the strong and tunable SOI in 2D systems. Additionally, gate-defined nanoconstrictions, such as quantum point contacts (QPCs) and quantum dots (QDs), have been fabricated and characterized. Moreover, a high-quality two-dimensional hole gas (2DHG) has been reported in undoped InSb, where ambipolar operation through global top gate sweeping is achieved. The characterization of this 2DHG may contribute to a better understanding of p-type narrow-band semiconductors. Finally, as the latest progress in Sb-based narrow-band semiconductor QWs, research on the ternary compound InAsSb will be briefly introduced.

2. MBE growth and the fabrication of InSb QW devices

Growing high-quality InSb QWs remains challenging, although a well-maintained MBE setup can enable precise epitaxy in ultra-high vacuum that minimizes background impurities. This is first because of the absence of high-quality, lattice-matched (semi)-insulating wafers as suitable substrates. For instance, while GaAs wafers are commonly used for III–V semiconductor epitaxy, they exhibit a lattice mismatch of about 14.6% with InSb. It is critical to overcome this large lattice mismatch and minimize dislocations to achieve smooth interfaces in heterostructures [29–33]. To address this, a carefully designed buffer system is commonly grown before the epitaxy of the active region. Here, as examples, we introduce two widely used buffer systems, aiding the growth of high-mobility InSb QWs for different experimental purposes.

As reported in [34], a typical InSb QW can be grown on a semi-insulating GaAs (100) substrate with a thick buffer on the substrate side. After a 100 nm thick GaAs smoothing layer, a 100 nm thick AlSb layer was grown. Subsequently, a 4 μm thick $In_{0.92}Al_{0.08}Sb$ layer was grown to serve as the virtual substrate and also the bottom barriers of the InSb QW. Following the growth of the InSb layer, the active layer of this heterostructure, $In_{0.92}Al_{0.08}Sb$ was grown as the top barrier of the QW. The significance of the thick $In_{0.92}Al_{0.08}Sb$ buffer lies in overcoming the mismatch and isolating dislocations. Therefore, reducing its thickness compromises the mobility of the 2DEG in the QW. With this buffer design, the achieved mobility has achieved $\sim$200 000 $cm^2\,Vs^{-1}$, while the density is $\sim 2 \times 10^{11}\,cm^{-2}$.

Instead of relying solely on a thick layer of InAsSb to overcome the lattice mismatching, Lehner *et al* [35], designed a buffer system with 6.1 Å -family intermediate layers and superlattices. Using a GaAs (100) wafer, they made a transition from GaAs to AlSb or GaSb with careful control of the growth temperature. Then, they grew the second intermediate buffer with InAlSb/InSb superlattices, followed by the growth of the active region. Surface morphology analysis verified that the interlayers and superlattices contribute to filtering threading dislocations, and the GaSb intermediate buffer provides a smoother surface. Applying the design of the second intermediate buffer, the InSb QW can be grown on a GaSb (100) wafer, eliminating the need for a transition from GaAs to GaSb. Using this buffer system, the electron mobility has been promoted to $\sim$349 000 $cm^2\,Vs^{-1}$. Furthermore, Shi *et al* [36, 37] carefully analyzed the effects of the GaAs substrate off-cut and achieved a defect-free surface in InSb/InAlSb heterostructure. Based on this approach, the mobility of InSb 2DEG has been promoted to $\sim$380 000 $cm^2\,Vs^{-1}$ in recent growth [38].

In general, dopants are necessary to obtain a conductive InSb QW. Both Te and Si can work as n-type dopants in the InAlSb barriers of InSb QWs, and Si is more commonly used now. Remote doping is widely adopted to reduce scattering [34, 35, 39–41]. The dopant density is crucial for achieving a high-quality single-channel system. For instance, if the dopant density is too high, the layer where the Si atoms are introduced will be conducting, forming another 2DEG which is in parallel to the InSb QW [42]. Furthermore, a largely asymmetric doping in the top and bottom InAlSb barriers may skew the QWs, making the effective width of the QW much smaller [43].

Unlike other semiconductor materials, the micro/nano fabrication of InSb QW devices is more challenging for at least two reasons. First, due to the narrow band gap, there is only a very small Schottky barrier between InSb and metals. Therefore, achieving a wide range of gate tunability with Schottky gates is unfeasible. Thereofore, a high-quality dielectric layer is needed between the QW surface and the top gate [44]. Second, the thermal budget (the highest processing temperature the material can sustain) of InSb QWs is only between 150 and 180 °C, which is much lower than those of Si and GaAs. Higher temperatures or heating processes longer than 1.5 h may cause the degrading of InSb QWs due to the

migration of Sb atoms [34, 45]. This small thermal budget imposes a critical requirement on the process of InSb QWs in the growth of the dielectric layer and adding ohmic contacts. Thanks to the development of the atomic layer deposition (ALD) technique, recipes for growing Al_2O_3 and HfO_2 dielectric layers at low temperatures (between 120 and 180 °C) are now available and reliable in many labs [34, 40, 46]. Compared with Al_2O_3, HfO_2 has the advantage of a lower trap density at the interface and a larger dielectric constant [34]. Nevertheless, Al_2O_3 is still widely used as it is more accessible and can be grown at lower temperatures (between 120 and 150 °C) [42, 47]. With the aid of the high-quality dielectric materials, the tunability of carrier density has been increased from a range from 1.8 to 2.6×10^{11} cm^{-2} [41] to a range from pinch-off to $\sim 5 \times 10^{11}$ cm^{-2} [40, 46, 48], higher than which the second subband or the interface scattering must be considered. The technique of making ohmic contacts on InSb QWs is more mature now. Although high-temperature annealing like in Si and GaAs is impossible, a low contact resistance ($\sim$ kΩ) is achievable with the cleaning of the surface of fresh QWs. Metals like Ti/Au or Ge/Ni/Au can diffuse into the InSb layer during the process later on at low temperatures [34, 48].

Although the pinch-off of the InSb 2DEG in the QW is achieved, the electrical stability is not satisfactory, posing difficulties in realizing nanoconstrictions. For example, the channel that has been pinched off with a top gate will turn conductive again within minutes. This issue has been reported in many groups with independent growth and micro/nano fabrication processes [47, 49, 50]. Solving this issue requires optimization from both the MBE growth and the device fabrication.

First, it is accepted that this instability may be due to the Si-doping in the InAlSb barrier. Regarding this issue, undoped InSb QWs are used, where the 2DEGs are induced with a global top gate covering both the contacts and the mesa [45]. With the elimination of Si-doping, a stable carrier density is achieved near the pinch-off, and nanoconstrictions like QDs are characterized [47]. However, as reported in other publications, the gate-defined 2DEGs and 2DHGs in undoped InSb QWs show more hysteresis during the large-range sweeping of the top gate voltage [48]. This implies that the screening and charging effects in InSb/InAlSb heterostructures and dielectric layers may still need further study for a better understanding.

Additionally, as reported by Bergeron *et al* [50], the instability of the InSb QWs could also be related to the Al in the upper barrier of InAlSb. According to this, the surface InSb QW is more stable than the QW with an InAlSb top barrier. Looking ahead, we expect that further optimization of heterostructure growth and device processing will enhance device stability, paving the way for more elaborate nanostructures based on InSb QWs.

3. Quantum transport in two-dimensional electron gases in InSb QWs

The high quality of InSb 2DEG allows for the quantum transport characterization of its unique properties, including the small effective mass and the large g-factor. Moreover, the gate tunability of the charge density has provided deeper insights into, for example, the Rashba SOI and its underlying scattering mechanisms.

Integer quantum Hall effects and Shubnikov-de Haas (SdH) oscillations in high-quality InSb QWs have been extensively reported [7, 34, 39, 40]. Precise measurements in moderate magnetic fields (around 1 T) have revealed a beating pattern in the SdH oscillations, indicating a zero-field spin-splitting caused by the large SOI [7]. Additionally, this large SOI has also been characterized by measurements of weak localization (WL) and weak antilocalization (WAL) effects in small magnetic fields [6]. In general, the strength of the SOI can be described by the spin-orbit coefficient α_{SO}, which is defined as $\alpha_{SO} = \Delta_{SO}/2k_F$. Here Δ_{SO} is the spin-orbit energy, and k_F presents the Fermi wave vector. In the undoped InSb QWs, where the asymmetry of the wave function can be enhanced with applied electric field, α_{SO} is tuned by the top gate voltage [45, 48]. Recently, in the work by Bergeron *et al* [50], a larger SOI has been reported in a surface InSb QW. Because of an even stronger asymmetry in the growth direction, α_{SO} is measured to be as large as 110 meVÅ.

The effective electron mass of 2DEGs in InSb QWs can be measured by analyzing the temperature dependence of SdH oscillations and the results agree well with $k \cdot p$ theory calculations [51, 52]. While the effective mass in the bulk material is calculated to be $\sim 0.014\, m_e$, the confinement in the growth direction increases the band gap effectively, leading to a larger effective mass in QWs. Consequently, the typical effective mass of electrons in InSb QWs with a typical width between 20 and 30 nm is approximately $0.016 \sim 0.02\, m_e$ [42, 45, 51, 52]. Despite the substantial non-parabolicity of the band in narrow-band semiconductor materials in bulk, the density-dependence of the effective mass remains negligible in the low-density regime where quantum transport experiments are conducted [42, 45].

Performing magneto-transport experiments in InSb QWs also allows a precise measurement of the effective g-factor using the so-called coincidence method [53, 54]. The Zeeman splitting depends on the total magnetic field, while the Landau level space depends on the perpendicular magnetic field. Therefore, the ratio r between the Zeeman and the Landau level splitting can be changed by changing the tilt angle θ, which is the angle between the sample normal and the magnetic field.

The results of coincidence measurements in different publications are similar. The dependence of the g-factor on the spin polarization P is of the most interest. Here, P can be calculated as $P = r/\nu$, where ν is the filling factor [45, 50, 51, 55]. In the regime where P is small, the g-factor closely agrees with $k \cdot p$ theory calculations. When P is much larger, the g-factor is enhanced by exchange interactions. Interestingly, in the density regime of the reported measurements , the effective g-factor also increases with carrier density, and the enhancement of the g-factor becomes more pronounced at higher carrier densities [45, 50]. This observation is the opposite of what is known in the diluted 2DEG of GaAs [56]. This difference may be because InSb QWs hold a rather small electron-electron interaction but a much larger SOI. Therefore, we can indeed

expect a larger g^* due to a stronger SOI when the carrier density is higher. Additionally, signatures of quantum Hall Ising ferromagnetism have been found in coincidence measurement where the Zeeman energy equals the Landau energy [45, 57].

Until now there have been no convincing reports on the observation of a fractional quantum Hall effect (FQHE) in InSb. FQHEs may be naively expected for the high mobilities which can be achieved in this system. However, the absence of FQHEs in InSb QWs might be most probably attributed to the small electron-electron interactions and the high kinetic energy of electrons in InSb. Therefore, the quality of InSb QWs should be further optimized to reach a regime where electron-electron interaction becomes visible.

To reach this aim, a comprehensive study of the scattering mechanisms can guide us towards further growth optimization. Across a wide range of carrier densities, the electron mobility is observed to be proportional to the carrier density, suggesting that the background impurity scattering is dominant [34, 45]. Calculations estimate that the density of background impurities is approximately $10^{17}\,\mathrm{cm}^{-3}$ in InSb QWs, which is significantly higher than in GaAs and InAs QW systems [48, 58, 59]. Therefore, reducing background impurities is the next step toward achieving higher mobility in InSb QWs.

4. Nanoconstrictions based on n-type InSb QWs

With a foundational understanding of the quantum transport of 2DEG and the preparation of device fabrication technology, exploring InSb-QW-based nanoconstrictions presents an intriguing avenue for further study in InSb quantum devices. As the most fundamental nanoconstrictions, both 1D QPC devices and 0D QD devices work in the regime of ballistic transport, where the mean free path is larger than the length of the device [60]. With the improvement of the sample quality, the mean free path of InSb 2DEG in QWs has been larger than $\sim$1 μm, which easily exceeds the typical geometric size of a QPC or QD device ($\sim$100 nm). However, as previously discussed, carrier density instability poses a significant obstacle to achieving high-quality nanoconstrictions. Resolving this issue of time-dependent device characteristics is the primary focus.

A QPC is obtained through the confinement of a 1D channel in the ballistic transport regime. For a long time, this 1D channel in InSb QWs was achieved with the aid of chemical etching. For instance, Goel *et al* [61] demonstrated quantization of conductance in a chemically etched 1D channel, revealing signatures of current focusing [62]. Qu *et al* [63] reported a stable QPC defined by a combination of chemical etching and a local top gate, measuring the g-factor to be $\sim$26 in-plane and $\sim$52 out-of-plane. Similar results were observed by Masuda *et al* [64]. There, the pinch-off is achieved with chemical etching-defined trench gates. While these etching-defined structures enable the study of quantum states in a 1D system, this etching method may introduce scattering centers at structure edges, limiting device quality. Moreover, the etching step adds complexity to the design and processing of integrated nanodevices. Before we could solve this issue completely by optimizing the growth of heterostructure and the ALD process, a stable purely gate-defined QPC has been achieved by optimizing the measurement protocol. The QPC can be dynamically stabilized with a special procedure for sweeping the gate voltage, enabling successive measurements with nearly identical electronic conditions [49]. Without chemical etching, this QPC takes advantage of the high quality of the InSb QWs. The main measurement results are presented in figure 1. Well-defined conductance plateaus are observed, and the subband structure of the QPC is extracted from finite-bias measurements. The Zeeman splitting is measured in both in-plane and out-of-plane magnetic fields. The in-plane g-factor is measured to be $\sim$40, and the out-of-plane g-factor is measured to be $\sim$50. The larger g-factor out-of-plane could be because of the enhancement of electron-electron interaction in a low-density regime. However, since there is no observable signature related to strong electron-electron interactions, this interpretation still needs more support from investigating QPCs with higher quality.

In comparison to QPC devices, achieving higher electronic stability is more imperative for QD devices. This means that the time-dependence of the electronic characteristics of the 2DEG should be negligible for hours, and even for days. Merely optimizing the measurement protocol is unlikely to meet this requirement. In an initial attempt, Kelush *et al* [47] successfully defined a stable QD on an undoped InSb QW. The device structure and the main results are shown in figure 2. Despite the QWs being insulating without doping, 2DEGs were induced with a global top gate covering both contacts and the mesa. The QD device demonstrated stability for hours, allowing measurement of the g-factor. The substantial g-factor of $\sim$30 facilitated the singlet-triplet transition at a significantly low magnetic field of 0.3 T. Compared with QD devices defined on other QW systems, such as in GaAs and Ge, the quality of the QD based on InSb QWs is still not satisfactory [65, 66]. There are still lots of phenomena that can be revealed to show the potential advantages of manipulating spin qubits in this strong SOI system. For instance, the excited states in artificial atoms and spin states in few-electron regimes need to be obtained [67]. This requires a better quality of the InSb QWs and a more sophisticated design of the nanostructures.

5. p-type InSb QWs

As previously reported, n-type InSb exhibits a near-parabolic band structure with a large SOI and g-factor. In contrast, for low-dimensional systems, p-type InSb, similar to other p-type III–V compounds, the band structures are predicted to be more complicated than their n-type counterparts. In general, they strongly depend on the dimensions, shape of the potential well, global or local strain fields, SOI, and carrier confinement [68–70]. Due to the less developed growth and processing methods for p-type InSb, studies on p-type InSb remain scarce. There are few publications in this topic. For instance, the polarity of InSb nanowires can be changed from n-type to p-type using a global back gate, and quantum transport measurements

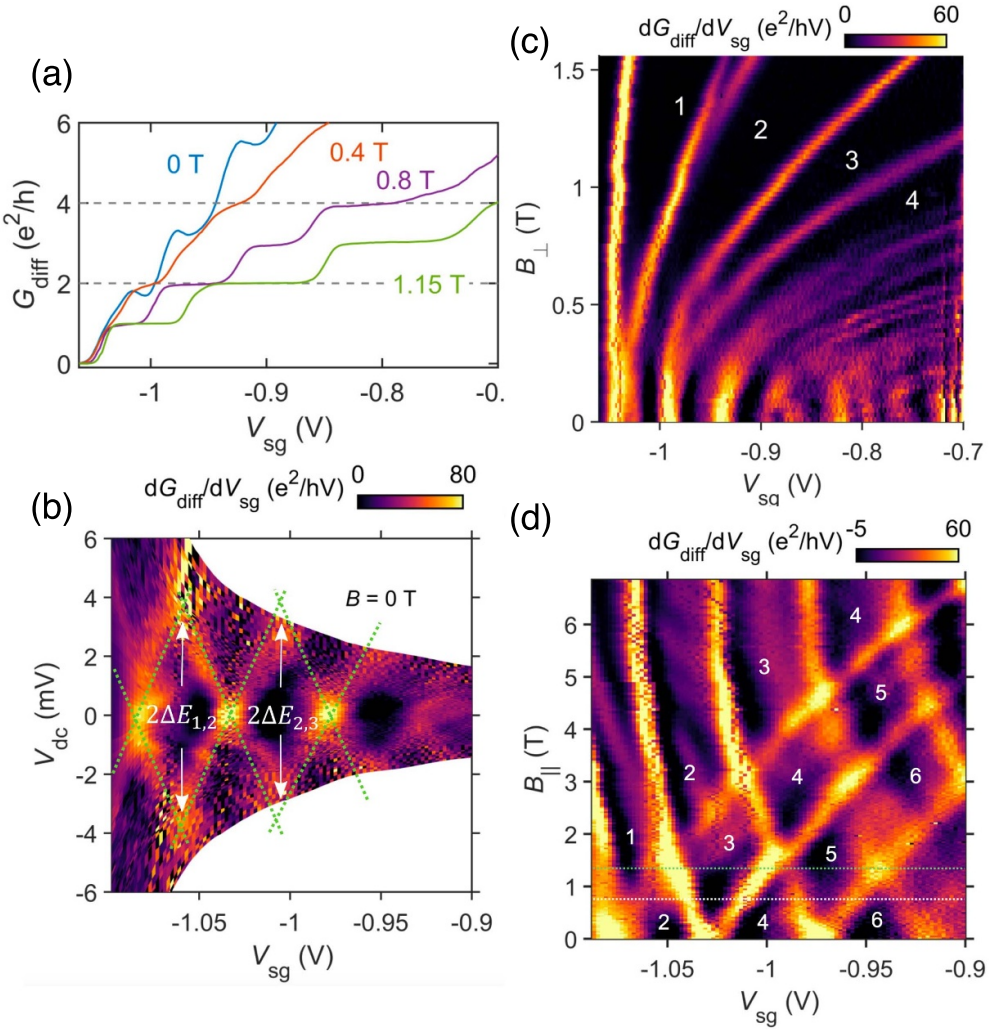

Figure 1. Measurement results of a gate-defined InSb QW QPC. (a) Differential conductance G_{diff} as a function of split gate voltage V_{sg} and the out-of-plane magnetic field $B_\perp$. Increasing the magnetic field, the spin-splitting is observed, and the conductance plateaus move towards the correct value (multiple of conductance quantum e^2/h). (b) Finite bias spectroscopy showing the transconductance $\mathrm{d}G_{\text{diff}}/\mathrm{d}V_{\text{sg}}$ as a function of V_{sg} and the DC voltage drop across the QPC V_{dc}. The energy spacings of the quantum state can be read out through the dimension of the diamond patterns, guided with the green dashed line. (c) Transconductance $\mathrm{d}G_{\text{diff}}/\mathrm{d}V_{\text{sg}}$ as a function of V_{sg} and $B_\perp$. Both magnetic depopulation and spin splitting are visible. The corresponding values of G_{diff} are labeled on the dark regions. (d) Transconductance $\mathrm{d}G_{\text{diff}}/\mathrm{d}V_{\text{sg}}$ as a function of V_{sg} and $B_{||}$. The white and green dashed lines show the magnetic fields where both even and odd multiples of e^2/h and only odd multiples of e^2/h conductance plateaus are visible, respectively. Reproduced from [49]. CC BY 4.0.

have been conducted on this device [71]. InSb transistors operating in both p- and n-type regimes at room temperature have also been reported [72]. Hindered by both material quality and device design limitations, important properties of p-type InSb, such as scattering mechanisms, effective mass, g-factor, and SOI, have not been precisely characterized.

The first attempt for transport study on p-type InSb QW is reported in [70]. Instead of Si-doping, C-doping was employed in the InAlSb barrier to convert the polarity to p-type. At 4.2 K, the mobility of this 2DHG ranged from 20 000 to 55 600 $\mathrm{cm^2\,Vs^{-1}}$, with the density tuned by varying the density of C dopants. Utilizing standard magneto-transport measurements, InSb 2DHG exhibited SdH oscillations and quantum Hall effects in magnetic fields between 1 and 8 T. The transport measurements indicated a single conductive channel, and a small hole effective mass of 0.017 to 0.083 m_e was obtained through cyclotron resonance measurements. This work suggested that the effective mass might depend on strain and carrier density in p-type InSb QWs.

As we discussed earlier, InSb has the smallest band gap among all III–V binaries, and Ti/Au can serve as suitable ohmic contacts for both p-type and n-type InSb [24]. Consequently, both 2DEG and 2DHG can be induced with an electric field in a single InSb QW device [48]. As shown in figure 3, an InSb QW is transformed from n-type to p-type by sweeping the top gate voltage from positive to negative regimes. The two-terminal conductance becomes zero between these two conductive regimes, indicating that the Fermi level resides in the band gap. Furthermore, both the 2DHG and 2DEG hold high mobility.

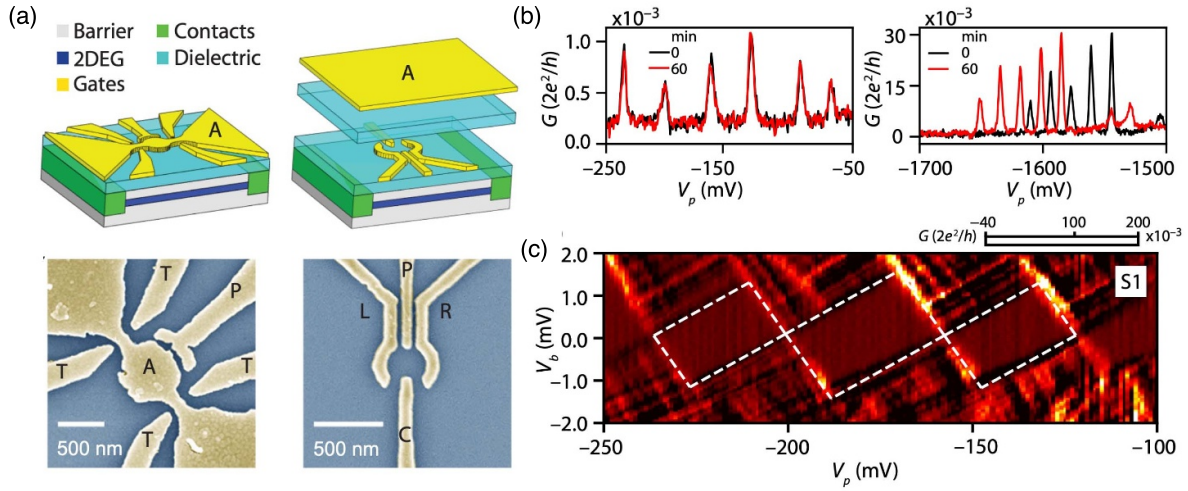

Figure 2. Gate-defined QD on InSb QW. (a) Upper panel: a sketch of the single-layer (left) and the double-layer types (right) design. A positive voltage is applied to gates A to populate charge carriers, while the other gates are energized with negative voltages. Bottom panel: A false-color scanning electron micrograph of the single-layer dot (left) and the double-layer dot prior to the second gate-layer deposition (right). (b) A comparison between the QDs based on undoped (left) and doped (right) InSb QWs. The time dependence of the coulomb resonance shows the undoped QD holds a much better stability. (c) Charge-stability diagrams for the QD with double-layer gates. Reprinted (figure) with permission from [47], Copyright (2020) by the American Physical Society.

On the one hand, achieving ambipolar operations in a semiconductor is meaningful because the presence of high-quality n- and p-type carriers is fundamental to today's complementary metal-oxide-semiconductor technology. On the other hand, the gate-defined 2DHG in undoped InSb QW provides an opportunity to investigate the quantum transport in p-type narrow-band semiconductors. As shown in figures 4(a) and (b), the effective mass of InSb 2DHG was measured using the temperature dependence of SdH oscillations. The effective mass of 2DHG in InSb QW is small, and it increases from 0.03 to 0.057 m_e with the carrier density rising from 3.1 to $4.85 \times 10^{11}\,\mathrm{cm}^{-2}$. The density-dependent effective mass indicates significant band non-parabolicity. Compared to the effective mass of holes in bulk InSb material, this work reveals a slightly larger value than the effective mass of the light holes ($0.015\,m_e$) but a much smaller value than the effective mass of the heavy holes ($\sim 0.43\,m_e$) [1]. This suggests that the band structure of p-type InSb may hold similarities to p-type GaAs, where the light-hole heavy-hole degeneracy at the Γ point lifted due to confinement in the growth direction. And theoretical predictions propose that the in-plane effective mass of the heavy-hole band is smaller than that of the light-hole band (mass inversion) [73].

This undoped structure also exhibits strong and tunable Rashba SOI in both 2DHG and 2DEG, which can be probed with WAL measurements in small magnetic fields. Due to the larger asymmetry along the growth direction, the SOI coefficient α_{SO} of the 2DEG is much larger than those in previous reports [45]. Here, α_{SO} is tunable from 34 to 91 meVÅ with increasing electron density. Additionally, as expected, the 2DHG of InSb QW demonstrates an even stronger SOI. As shown in figure 4(c), the $\rho_{xx}(B) - B$ diagram transitions from the WL regime to the WAL regime, indicating a large tunability of SOI strength. A rough estimation, using the parabolic band approximation, suggests that the ratio between SOI energy Δ_{SO} and Fermi energy E_{F} increases from 5.2% to 8.2%.

Moreover, the effective g-factor of the 2DHG exhibits strong density dependence based on coincidence measurements. In the low-density regime (figure 4(d)), the ratio between Zeeman energy and Landau energy can be increased to $\sim$1 within the measurement range. There, the longitudinal resistance $\rho_{xx}(B)$ corresponding to odd filling factors in SdH oscillations changes to local minima. With this tilt angle θ, the g-factor is calculated to be $\sim$15, close to the g-factor of bulk p-type InSb. However, in a high-density regime (figure 4(e)), there is no obvious dependence of $\rho_{xx}(B)$ on θ. Since the SOI of the 2DHG is stronger in the high-density regime, it could be expected that the spin of holes is locked with the orbits due to the larger SOI [74, 75].

The up-to-date characterization of the 2DHG in InSb QWs reveals vast potential for further study in narrow-band semiconductor physics. Due to the small band gap, the strong virtual coupling between the conduction and valence bands makes the band structure and the quantum properties a 'touchstone' for band calculation methods [2]. It is crucial to note that the published data do not fully align with theoretical calculations. For instance, magneto-transport measurements in both doped and undoped structures consistently show that only one band is populated, and there is no observable splitting of the heavy-hole bands into the so-called 'heavy-heavy-hole' band and the 'light-heavy-hole' band, as seen in GaAs 2DHGs [76, 77]. Additionally, the measured effective mass is much smaller than the calculated value [69, 78]. Generally, the

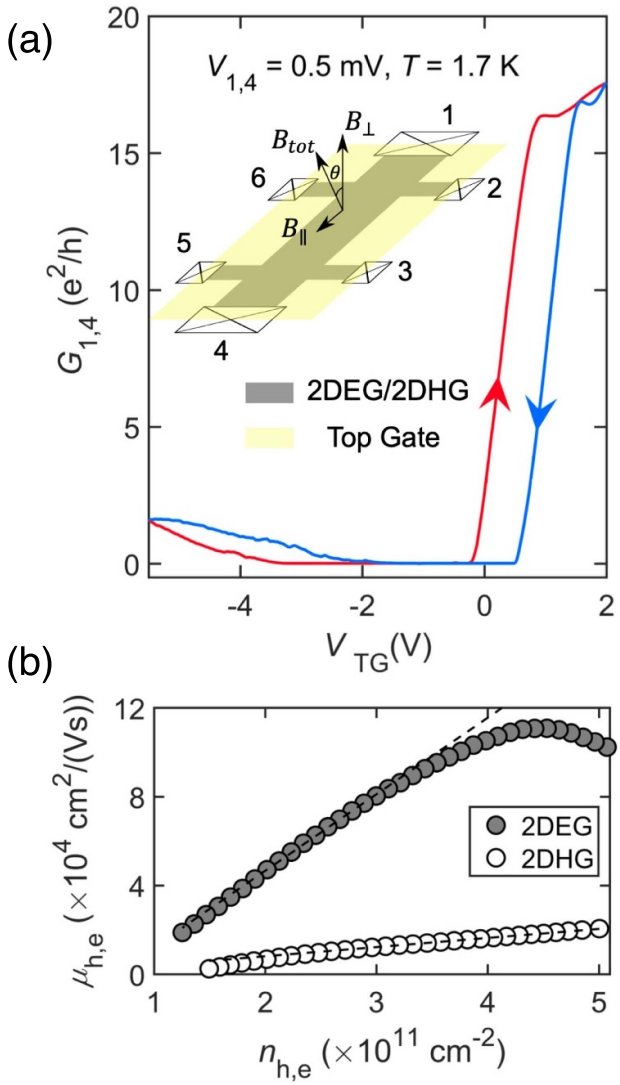

Figure 3. (a) Field effect in the Hall bar based on undoped InSb QW. Two-terminal conductance $G_{1,4}$ measured between contacts 1 and 4 vs. top gate voltage V_{TG}. The blue and red traces show the down- and up-sweep, respectively. Inset: a schematic diagram of the Hall bar sample and the definition of tilt angle θ. (b) The mobilities vs. densities for both 2DHG and 2DEG. The dashed lines are linear fits. Reproduced from [48]. CC BY 4.0.

details of the band structures of p-type semiconductors are not well understood compared to n-type semiconductors, and there are very few publications about p-type InSb. Therefore, we expect more efforts to be taken, both theoretically and experimentally, to better understand narrow-band semiconductor materials. Here, we also need to point out that gate-defined 2DHGs still have drawbacks for studying p-type semiconductors. First, there are relatively higher requirements for the quality of the heterostructures and the dielectric layers. Without these, polarity will not easily change to p-type with an electric field. Second, since the 2DHG can only be very close to the surface, the mobility of the gate-defined 2DHG is limited. So, the development of doped p-type InSb QWs is still desired. Furthermore, as a perspective, the high-quality InSb 2DHG with strong and tunable SOI and a large g-factor could serve as a new platform for spin-based quantum information processing and research on Majorana-Andreev physics.

6. InAsSb: aiming for an even smaller band gap

Despite InSb having a small band gap, this gap can be further reduced by introducing As atoms into InSb, forming an InAsSb ternary compound. Indeed, experiments in the bulk have confirmed a strong negative bowing of the band gap with a bowing coefficient of ∼0.8 eV, resulting in a minimum band gap of 0.1 eV when the Sb composition is close to 63% [79, 80]. This narrower bandgap has sparked increased interest in infrared optoelectronic devices and quantum transport studies. In particular, InAsSb is gaining attention due to its smaller effective mass in the conduction band, larger SOI, and a significant effective g-factor, even when compared to InSb.

Several reports have detailed the MBE growth and characterization of InAsSb materials in bulk and two-dimensional (2D) structures [81, 82]. Optical measurements on bulk material have revealed an effective g-factor exceeding 100 when the Sb composition approaches 63% [83]. Furthermore, the g-factor has been reported to be tunable between 20 and 110 in InAsSb/InSb superlattices by altering the superlattice period [84]. Additionally, this superlattice exhibits signatures of a Dirac energy spectrum and inverted band gap, as observed with angle-resolved photoemission spectroscopy measurements [85, 86].

The successful growth of InAsSb has enabled quantum transport studies in InAsSb QWs. Recent studies [43, 82] report mobilities of around 10^4 cm^2 Vs^{-1}, which is still considerably lower than that of comparable InSb QWs. This can be mainly attributed to alloy scattering and the challenges of homogeneously mixing As atoms into InSb. Nevertheless, the quality achieved so far for InAsSb still allows for the investigation of its exceptional quantum properties. For example, Metti *et al* [82] observed a stronger SOI in InAsSb through the beating of SdH oscillations, even with an As composition only as high as 19%. This result aligns with characterizations through WAL in InAsSb surface QWs [87]. Through magnetoresistance transport measurements, the effective mass of InAsSb was confirmed to be smaller than that in InSb, with the effective mass decreasing as the Sb composition approaches 63%. Moreover, the g-factor of InAsSb was reported to be larger than that of InSb in a study by Bal *et al* [43], despite both InSb and InAsSb QWs being significantly skewed due to the large asymmetry induced by Si-doping on both sides of the barrier.

Quantum transport studies in nanoconstrictions based on InAsSb QWs are undertaken. For instance, Metti *et al* reported a gate-defined QD based on an undoped InAsSb QW [88]. Despite the As ratio being only 13%, the QD exhibited a larger g-factor and strong Rashba SOI. Additionally, since the electrons in InAsSb are gate-induced, the SOI is tunable with a global top gate.

InAsSb is now regarded as a promising platform for Majorana devices. Compared to InSb, it has a stronger SOI

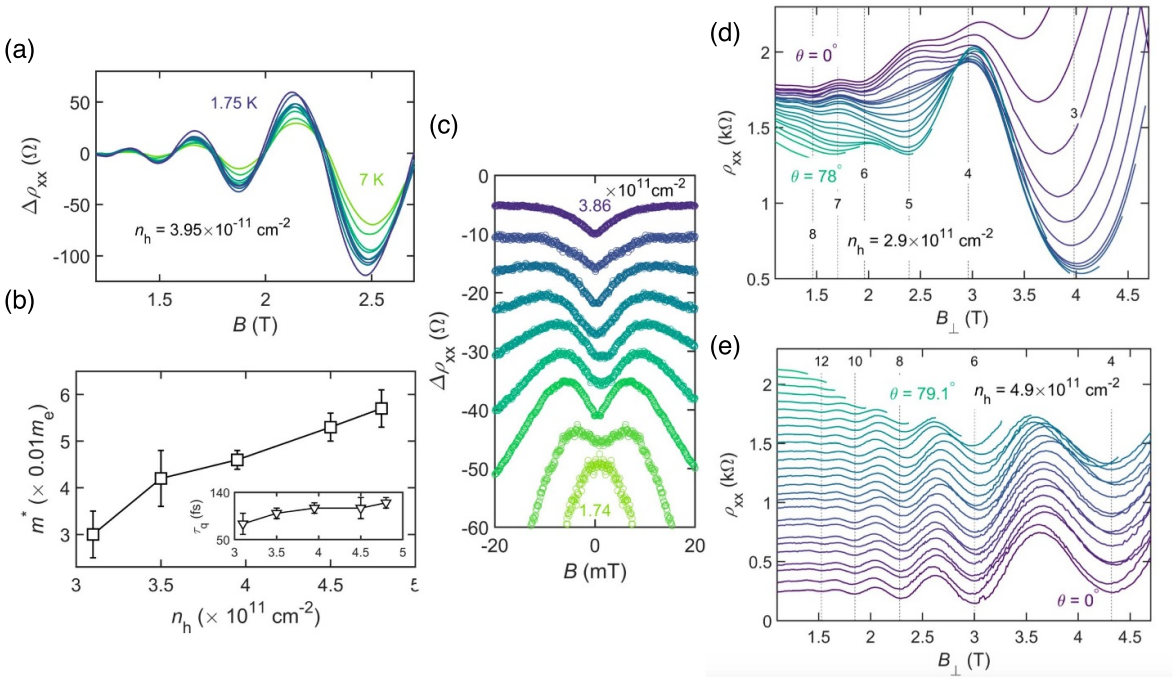

Figure 4. Quantum transport in InSb 2DHG. (a) Temperature dependence of SdH oscillations with hole density $n_h = 3.95 \times 10^{11}$ cm^{-2}. The effective mass is calculated with the Ando formula. (b) Effective mass as a function of carrier density, showing a large band nonparabolicity. Inset: Dependence of quantum lifetime of Landau states τ_q on n_h at 1.75 K. (c) Density dependence of WAL for 2DHG. Increasing hole density, the sample is tuned from WL to WAL, indicating an increased SOI. (d) and (e) The coincidence measurement of InSb 2DHG when hole densities are 2.9 and 4.9 × 10^{11} cm^{-2}, respectively. The filling factors are labeled with dashed lines. Reproduced from [48]. CC BY 4.0.

and a larger g-factor. Moreover, the introduction of As atoms makes it easier to achieve a strong coupling to in-situ grown aluminum on the surface. This induces the InAsSb beneath to become superconductive at low temperatures [89, 90]. Consequently, sophisticated nanostructures can be defined with standard process methods on a 2D Sb-based material system, providing more alternatives to explore Majorana physics in semiconductor-superconductor hybrid devices [87, 91, 92].

7. Conclusion and outlook

In summary, this review highlights recent advancements in quantum transport research on InSb QW devices. The growth of high-quality InSb heterostructures, coupled with advances in micro/nano fabrication techniques, has enabled a systematic exploration of the unique quantum properties exhibited by InSb in low-dimensional systems. Considering the challenges related to carrier density stability and electron mobility, we still expect continued advancements in growth and fabrication techniques to improve the quality of InSb devices. The investigation of InSb 2DHGs underscores the need for a deeper understanding of p-type narrow-band semiconductors in confined systems. The emerging field of InAsSb has garnered increased attention due to even smaller band gaps. Quantum transport experiments in InAsSb have revealed new interesting properties compared to InSb, positioning InAsSb as a promising platform for exploring novel quantum phenomena and serving as a foundation for topological quantum information processing.

Data availability statement

No new data were created or analysed in this study.

Acknowledgment

We acknowledge funding from QuantERA. This work was supported by the Swiss National Science Foundation through the National Center of Competence in Research Quantum Science and Technology. This work is also supported by HFML-RU/NWO-I, member of the European Magnetic Field Laboratory (EMFL). It is part of the research programme 'HFML-FELIX: a unique research infrastructure in the Netherlands. Matter under extreme conditions of intense infrared radiation and high magnetic fields' with Project Number 184.034.022 financed by the Dutch Research Council (NWO).

ORCID iDs

Zijin Lei https://orcid.org/0000-0002-1420-320X
Erik Cheah https://orcid.org/0000-0003-4240-8680
Rüdiger Schott https://orcid.org/0000-0002-9320-0313

Christian A Lehner https://orcid.org/0000-0002-7802-7719
Uli Zeitler https://orcid.org/0000-0002-5293-2673
Werner Wegscheider https://orcid.org/0000-0002-2138-5558
Thomas Ihn https://orcid.org/0000-0002-5587-6953
Klaus Ensslin https://orcid.org/0000-0001-7007-6949

References

[1] Roessler U, Madelung O and Schulz M 2000 *Landolt-Bernstein-Group III Condensed Matter* 41D (Springer)
[2] Vurgaftman I, áR Meyer J and áR Ram-Mohan L 2001 Band parameters for III–V compound semiconductors and their alloys *J. Appl. Phys.* **89** 5815–75
[3] Zhang T, Clowes S K, Debnath M, Bennett A, Roberts C, Harris J J, Stradling R A, Cohen L F, Lyford T and Fewster P F 2004 High-mobility thin InSb films grown by molecular beam epitaxy *Appl. Phys. Lett.* **84** 4463–5
[4] Kallaher R L, Heremans J J, Goel N, Chung S J and Santos M B 2010 Spin-orbit interaction determined by antilocalization in an InSb quantum well *Phys. Rev.* B **81** 075303
[5] Khodaparast G A, Doezema R E, Chung S J, Goldammer K J and Santos M B 2004 Spectroscopy of Rashba spin splitting in InSb quantum wells *Phys. Rev.* B **70** 155322
[6] Leontiadou M A *et al* 2011 Experimental determination of the Rashba coefficient in InSb/InAlSb quantum wells at zero magnetic field and elevated temperatures *J. Phys.: Condens. Matter* **23** 035801
[7] Gilbertson A M, Branford W R, Fearn M, Buckle L, Buckle P D, Ashley T and Cohen L F 2009 Zero-field spin splitting and spin-dependent broadening in high-mobility insb/$In_1 - x$ Al_x sb asymmetric quantum well heterostructures *Phys. Rev.* B **79** 235333
[8] Vdovin A V and Skok E M 1986 Precise measurement of the free electron g-factor in InSb *Physica Status Solidi* b **136** 603–13
[9] Ashley T, Dean A B, Elliott C T, Pryce G J, Johnson A D and Willis H 1995 Uncooled high-speed InSb field-effect transistors *Appl. Phys. Lett.* **66** 481
[10] Ueno K, Camargo E G, Katsumata T, Goto H, Kuze N, Kangawa Y and Kakimoto K 2013 InSb mid-infrared photon detector for room-temperature operation *Jpn. J. Appl. Phys.* **52** 092202
[11] Žutić I, Fabian J and Sarma S D 2004 Spintronics: fundamentals and applications *Rev. Mod. Phys.* **76** 323
[12] Oreg Y, Refael G and Von Oppen F 2010 Helical liquids and majorana bound states in quantum wires *Phys. Rev. Lett.* **105** 177002
[13] Riwar R P, Houzet M, Meyer J S and Nazarov Y V 2016 Multi-terminal Josephson junctions as topological matter *Nat. Commun.* **7** 1–5
[14] Stern A and Berg E 2019 Fractional Josephson vortices and braiding of majorana zero modes in planar superconductor-semiconductor heterostructures *Phys. Rev. Lett.* **122** 107701
[15] Ke C T *et al* 2019 Ballistic superconductivity and tunable π–junctions in InSb quantum wells *Nat. Commun.* **10** 1–6
[16] Peng Y, Pientka F, Berg E, Oreg Y and von Oppen F 2016 Signatures of topological josephson junctions *Phys. Rev.* B **94** 085409
[17] Fornieri A *et al* 2019 Evidence of topological superconductivity in planar josephson junctions *Nature* **569** 89–92
[18] Cheah E *et al* 2023 Control over epitaxy and the role of the InAs/Al interface in hybrid two-dimensional electron gas systems *Phys. Rev. Mater.* **7** 073403
[19] Haxell D Z *et al* 2023 Measurements of phase dynamics in planar Josephson junctions and squids *Phys. Rev. Lett.* **130** 087002
[20] Haxell D Z, Coraiola M, Sabonis D, Hinderling M, Kate S C T, Cheah E, Krizek F, Schott R, Wegscheider W and Nichele F 2023 Zeeman-and orbital-driven phase shifts in planar Josephson junctions *ACS Nano* **17** 18139–47
[21] Gül Onder, van Woerkom D J, van Weperen I, Car D, Plissard S R, Bakkers E P A M and Kouwenhoven L P 2015 Towards high mobility InSb nanowire devices *Nanotechnology* **26** 215202
[22] Nilsson H A, Caroff P, Thelander C, Larsson M, Wagner J B, Wernersson L-E, Samuelson L and Xu H Q 2009 Giant, level-dependent g factors in InSb nanowire quantum dots *Nano Lett.* **9** 3151–6
[23] Nilsson H A, Karlström O, Larsson M, Caroff P, Pedersen J N, Samuelson L, Wacker A, Wernersson L-E and Xu H Q 2010 Correlation-induced conductance suppression at level degeneracy in a quantum dot *Phys. Rev. Lett.* **104** 186804
[24] Nilsson H A, Deng M T, Caroff P, Thelander C, Samuelson L, Wernersson L-E and Xu H Q 2011 InSb nanowire field-effect transistors and quantum-dot devices *IEEE J. Sel. Top. Quantum Electron.* **17** 907–14
[25] de la Mata M, Leturcq R, Plissard S R, Rolland C, Magén C, Arbiol J and Caroff P 2016 Twin-induced InSb nanosails: a convenient high mobility quantum system *Nano Lett.* **16** 825–33
[26] Pan D, Fan D X, Kang N, Zhi J H, Yu X Z, Xu H Q and Zhao J H 2016 Free-standing two-dimensional single-crystalline InSb nanosheets *Nano Lett.* **16** 834–41
[27] Kang N, Fan D, Zhi J, Pan D, Li S, Wang C, Guo J, Zhao J and Xu. H 2018 Two-dimensional quantum transport in free-standing InSb nanosheets *Nano Lett.* **19** 561–9
[28] Xue J, Chen Y, Pan D, Wang J-Y, Zhao J, Huang S and Xu H Q 2019 Gate defined quantum dot realized in a single crystalline InSb nanosheet *Appl. Phys. Lett.* **114** 023108
[29] Wu S D, Guo L W, Li Z H, Shang X Z, Wang W X, Huang Q and Zhou J M 2005 Effect of the low-temperature buffer thickness on quality of InSb grown on gaas substrate by molecular beam epitaxy *J. Cryst. Growth* **277** 21–25
[30] Zhang X, Staton-Bevan A E, Pashley D W, Parker S D, Droopad R, Williams R L and Newman R C 1990 A transmission electron microscopy and reflection high-energy electron diffraction study of the initial stages of the heteroepitaxial growth of InSb on GaAs (001) by molecular beam epitaxy *J. Appl. Phys.* **67** 800–6
[31] Soderstrom J R, Cumming M M, Yao J Y and Andersson T G 1992 Molecular beam epitaxy growth and characterization of InSb layers on gaas substrates *Semicond. Sci. Technol.* **7** 337
[32] Mishima T D, Keay J C, Goel N, Ball M A, Chung S J, Johnson M B and Santos M B 2005 Effect of micro-twin defects on InSb quantum wells *J. Vac. Sci. Technol.* B **23** 1171–3
[33] Chung S J, Ball M A, Lindstrom S C, Johnson M B and Santos M B 2000 Improving the surface morphology of InSb quantum-well structures on GaAs substrates *J. Vac. Sci. Technol.* B **18** 1583–5
[34] Yi W *et al* 2015 Gate-tunable high mobility remote-doped InSb/In1-xAlxSb quantum well heterostructures *Appl. Phys. Lett.* **106** 142103
[35] Lehner C A, Tschirky T, Ihn T, Dietsche W, Keller J, Fält S and Wegscheider W 2018 Limiting scattering processes in high-mobility InSb quantum wells grown on gasb buffer systems *Phys. Rev. Mater.* **2** 054601

[36] Shi Y, Gosselink D, Umansky V Y, Weyher J L and Wasilewski Z R 2017 Threading dislocations in MBE grown AlInSb metamorphic buffers: revealed and counted *J. Vac. Sci. Technol.* B **35** 02B112

[37] Shi Y 2021 Molecular beam epitaxial growth of InSb quantum well heterostructures for applications in topological quantum computing *PhD Thesis* University of Waterloo (available at: http://hdl.handle.net/10012/17362)

[38] Cheah E 2023 Molecular beam epitaxy of InAs/Al and InSb heterostructures for hybrid semiconductor/superconductor devices *PhD Thesis* ETH Zurich

[39] Goldammer K J, Chung S J, Liu W K, Santos M B, Hicks J L, Raymond S and Murphy S Q 1999 High-mobility electron systems in remotely-doped InSb quantum wells *J. Cryst. Growth* **201-202** 753–6

[40] Uddin M M, Liu H W, Yang K F, Nagase K, Sekine K, Gaspe C K, Mishima T D, Santos M B and Hirayama Y 2013 Gate depletion of an InSb two-dimensional electron gas *Appl. Phys. Lett.* **103** 123502

[41] Pooley O J, Gilbertson A M, Buckle P D, Hall R S, Emeny M T, Fearn M, Halsall M P, Cohen L F and Ashley T 2010 Quantum well mobility and the effect of gate dielectrics in remote doped InSb/$Al_xIn_{1-x}Sb$ heterostructures *Semicond. Sci. Technol.* **25** 125005

[42] Lei Z, Lehner C A, Cheah E, Karalic M, Mittag C, Alt L, Scharnetzky J, Wegscheider W, Ihn T and Ensslin K 2019 Quantum transport in high-quality shallow InSb quantum wells *Appl. Phys. Lett.* **115** 012101

[43] Bal M E, Cheah E, Lei Z, Schott R, Lehner C A, Engelkamp H, Wegscheider W and Zeitler U 2023 Quantum Hall effect in InAsSb quantum wells at elevated temperatures *Phys. rev. res.* **6** 023259

[44] Orr J M S, Buckle P D, Fearn M, Storey C J, Buckle L and Ashley T 2007 A surface-gated InSb quantum well single electron transistor *New J. Phys.* **9** 261

[45] Lei Z *et al* 2022 High-quality two-dimensional electron gas in undoped InSb quantum wells *Phys. Rev. Res.* **4** 013039

[46] Uddin M M, Liu H W, Yang K F, Nagase K, Mishima T D, Santos M B and Hirayama Y 2012 Characterization of InSb quantum wells with atomic layer deposited gate dielectrics *Appl. Phys. Lett.* **101** 233503

[47] Kulesh I, Ke C T, Thomas C, Karwal S, Moehle C M, Metti S, Kallaher R, Gardner G C, Manfra M J and Goswami S 2020 Quantum dots in an InSb two-dimensional electron gas *Phys. Rev. Appl.* **13** 041003

[48] Lei Z, Cheah E, Krizek F, Schott R, Bähler T, Märki P, Wegscheider W, Shayegan M, Ihn T and Ensslin K 2023 Gate-defined two-dimensional hole and electron systems in an undoped InSb quantum well *Phys. Rev. Res.* **5** 013117

[49] Lei Z, Lehner C A, Cheah E, Mittag C, Karalic M, Wegscheider W, Ensslin K and Ihn T 2021 Gate-defined quantum point contact in an InSb two-dimensional electron gas *Phys. Rev. Res.* **3** 023042

[50] Bergeron E A, Sfigakis F, Shi Y, Nichols G, Klipstein P C, Elbaroudy A, Walker S M, Wasilewski Z R and Baugh J 2023 Field effect two-dimensional electron gases in modulation-doped InSb surface quantum wells *Appl. Phys. Lett.* **122** 012103

[51] Yang K F, Liu H W, Mishima T D, Santos M B, Nagase K and Hirayama Y 2011 Nonlinear magnetic field dependence of spin polarization in high-density two-dimensional electron systems *New J. Phys.* **13** 083010

[52] Lei Z *et al* 2020 Electronic g factor and magnetotransport in InSb quantum wells *Phys. Rev. Res.* **2** 033213

[53] Schumacher H W, Nauen A, Zeitler U, Haug R J, Weitz P, Jansen A G M and Schäffler F 1998 Anomalous coincidences between valley split Landau levels in a Si/SiGe heterostructure *Physica* B **256–258** 260–3

[54] Brosig S, Ensslin K, Jansen A G, Nguyen C, Brar B, Thomas M and Kroemer H 2000 InAs-AlSb quantum wells in tilted magnetic fields *Phys. Rev.* B **61** 13045–9

[55] Nedniyom B, Nicholas R J, Emeny M T, Buckle L, Gilbertson A M, Buckle P D and Ashley T 2009 Giant enhanced g-factors in an InSb two-dimensional gas *Phys. Rev.* B **80** 125328

[56] Zhu J, Stormer H L, Pfeiffer L N, Baldwin K W and West K W 2003 Spin susceptibility of an ultra-low-density two-dimensional electron system *Phys. Rev. Lett.* **90** 056805

[57] Chokomakoua J C, Goel N, Chung S J, Santos M B, Hicks J L, Johnson M B and Murphy S Q 2004 Ising quantum Hall ferromagnetism in InSb-based two-dimensional electronic systems *Phys. Rev.* B **69** 235315

[58] Tschirky T, Mueller S, Lehner C A, Faelt S, Ihn T, Ensslin K and Wegscheider W 2017 Scattering mechanisms of highest-mobility InAs/$Al_xGa_{1-x}Sb$ quantum wells *Phys. Rev.* B **95** 115304

[59] Chung Y J, Wang C, Singh S K, Gupta A, Baldwin K W, West K W, Shayegan M, Pfeiffer L N and Winkler R 2022 Record-quality gaas two-dimensional hole systems *Phys. Rev. Mater.* **6** 034005

[60] Ihn T 2010 *Semiconductor Nanostructures: Quantum States and Electronic Transport* (Oxford University Press)

[61] Goel N, Graham J, Keay J C, Suzuki K, Miyashita S, Santos M B and Hirayama Y 2005 Ballistic transport in InSb mesoscopic structures *Physica* E **26** 455–9

[62] Dedigama A R, Deen D, Murphy S Q, Goel N, Keay J C, Santos M B, Suzuki K, Miyashita S and Hirayama Y 2006 Current focusing in InSb heterostructures *Physica* E **34** 647–50

[63] Qu F *et al* 2016 Quantized conductance and large g-factor anisotropy in InSb quantum point contacts *Nano Lett.* **16** 7509–13

[64] Masuda T, Sekine K, Nagase K, Wickramasinghe K S, Mishima T D, Santos M B and Hirayama Y 2018 Transport characteristics of InSb trench-type in-plane gate quantum point contact *Appl. Phys. Lett.* **112** 192103

[65] Hanson R, Kouwenhoven L P, Petta J R, Tarucha S and Vandersypen L M K 2007 Spins in few-electron quantum dots *Rev. Mod. Phys.* **79** 1217–65

[66] Burkard G, Ladd T D, Pan A, Nichol J M and Petta J R 2023 Semiconductor spin qubits *Rev. Mod. Phys.* **95** 025003

[67] Leon R C C *et al* 2020 Coherent spin control of s-, p-, d-and f-electrons in a silicon quantum dot *Nat. Commun.* **11** 797

[68] Eisenstein J P, Störmer H L, Narayanamurti V, Gossard A C and Wiegmann W 1984 Effect of inversion symmetry on the band structure of semiconductor heterostructures *Phys. Rev. Lett.* **53** 2579–82

[69] Marcellina E, Hamilton A R, Winkler R and Culcer D 2017 Spin-orbit interactions in inversion-asymmetric two-dimensional hole systems: a variational analysis *Phys. Rev.* B **95** 075305

[70] Gaspe C K, Edirisooriya M, Mishima T D, Jayathilaka P A R D, Doezema R E, Murphy S Q, Santos M B, Tung L C and Wang Y-J 2011 Effect of strain and confinement on the effective mass of holes in InSb quantum wells *J. Vac. Sci. Technol.* B **29** 03C110

[71] Pribiag V S, Nadj-Perge S, Frolov S M, Van Den Berg J W G, Van Weperen I, Plissard S R, Bakkers E P A M and Kouwenhoven L P 2013 Electrical control of single hole spins in nanowire quantum dots *Nat. Nanotechnol.* **8** 170–4

[72] Radosavljevic M *et al* 2008 High-performance 40nm gate length InSb p-channel compressively strained quantum well field effect transistors for low-power (vcc= 0.5 v) logic applications *IEEE Int. Electron Devices Meeting* (IEEE) pp 1–4

[73] Winkler R 2003 *Spin-Orbit Coupling Effects in Twoi-Dimensional Electron and Hole Systems* (Springer)

[74] Shi Q, Zudov M A, Morrison C and Myronov M 2015 Strong transport anisotropy in ge/sige quantum wells in tilted magnetic fields *Phys. Rev.* B **91** 201301

[75] Pisoni R, Lee Y, Overweg H, Eich M, Simonet P, Watanabe K, Taniguchi T, Gorbachev R, Ihn T and Ensslin K 2017 Gate-defined one-dimensional channel and broken symmetry states in MoS_2 van der waals heterostructures *Nano Lett.* **17** 5008–11

[76] Habib B, Shayegan M and Winkler R 2009 Spin-orbit interaction and transport in GaAs two-dimensional holes *Semicond. Sci. Technol.* **24** 064002

[77] Nichele F, Pal A N, Winkler R, Gerl C, Wegscheider W, Ihn T and Ensslin K 2014 Spin-orbit splitting and effective masses in p-type gaas two-dimensional hole gases *Phys. Rev.* B **89** 081306

[78] Pryor C E and Pistol M-E 2005 Band-edge diagrams for strained III–V semiconductor quantum wells, wires and dots *Phys. Rev.* B **72** 205311

[79] Suchalkin S *et al* 2016 Electronic properties of unstrained unrelaxed narrow gap InAsxSb1-x alloys *J. Phys. D: Appl. Phys.* **49** 105101

[80] Svensson S P, Sarney W L, Hier H, Lin Y, Wang D, Donetsky D, Shterengas L, Kipshidze G and Belenky G 2012 Band gap of $InAs_{1-x}sb_x$ with native lattice constant *Phys. Rev.* B **86** 245205

[81] Sarney W L, Svensson S P, Xu Y, Donetsky D and Belenky G 2017 Bulk InAsSb with 0.1 eV bandgap on gaas *J. Appl. Phys.* **122** 025705

[82] Metti S, Thomas C, Xiao D and Manfra M J 2022 Spin-orbit coupling and electron scattering in high-quality $insb_{1-x}as_x$ quantum wells *Phys. Rev.* B **106** 165304

[83] Jiang Y, Ermolaev M, Moon S, Kipshidze G, Belenky G, Svensson S, Ozerov M, Smirnov D, Jiang Z and Suchalkin S 2023 g-factor engineering with InAsSb alloys toward zero band gap limit *Phys. Rev.* B **108** L121201

[84] Jiang Y, Ermolaev M, Kipshidze G, Moon S, Ozerov M, Smirnov D, Jiang Z and Suchalkin S 2022 Giant g-factors and fully spin-polarized states in metamorphic short-period InAsSb/InSb superlattices *Nat. Commun.* **13** 5960

[85] Suchalkin S *et al* 2020 Dirac energy spectrum and inverted bandgap in metamorphic InAsSb/InSb superlattices *Appl. Phys. Lett.* **116** 032101

[86] Suchalkin S *et al* 2018 Engineering dirac materials: metamorphic $InAs_{1-x}$ Sb_x/$InAs_{1-y}Sb_y$ superlattices with ultralow bandgap *Nano Lett.* **18** 412–7

[87] Moehle C M *et al* 2021 InSbAs two-dimensional electron gases as a platform for topological superconductivity *Nano Lett.* **21** 9990–6

[88] Metti S, Thomas C and Manfra M J 2023 Electronic g factor and tunable spin-orbit coupling in a gate-defined InSbAs quantum dot *Phys. Rev.* B **108** 235306

[89] Mayer W *et al* 2020 Superconducting proximity effect in InAsSb surface quantum wells with in situ Al contacts *ACS Appl. Electron. Mater.* **2** 2351–6

[90] Thomas C, Diaz R E, Dycus J H, Salmon M E, Daniel R E, Wang T, Gardner G C and Manfra M J 2019 Toward durable Al-InSb hybrid heterostructures via epitaxy of 2ml interfacial InAs screening layers *Phys. Rev. Mater.* **3** 124202

[91] Wang Q, Haaf S L D T, Kulesh I, Xiao Di, Thomas C, Manfra M J and Goswami S 2023 Triplet correlations in cooper pair splitters realized in a two-dimensional electron gas *Nat. Commun.* **14** 4876

[92] ten Haaf S L D *et al* 2023 A two-site Kitaev chain in a two-dimensional electron gas *Nature* **630** 329–34